

Radiative Cooling in Hot Humid Climates

Aubrey Jaffer

October 2006

Abstract

Passive radiative cooling of buildings has been an underachieving concept for decades. The few deployments have generally been in dry climates with low solar angles.

The greatest need for cooling is in the tropics. The high humidity endemic to many of these regions severely limits the passive cooling available per radiative area. To wrest temperature relief from humid climates, not just nocturnal cooling but solar irradiance, both direct and indirect, must be addressed.

This investigation explores the extent to which thermal radiation can be used to cool buildings in the tropics. It concludes that inexpensive materials could be fabricated into roof panels providing passive cooling day and night in tropical locations with an unobstructed view of sky.

Introduction

“European heatwave caused 35,000 deaths”[32] shows that cooling is not merely for comfort. Most people in tropical regions must endure high heat daily. Much illness and death result from exposure to insect-borne disease while dwellings are ventilated or too hot to occupy.

A sizable fraction of the electricity currently generated is used for cooling and refrigeration. It is ironic that in order to be cool we contribute to global warming. That infinite 3 K heat sink we call the universe holds promise of opportunities to cool more efficiently.

Black Body Radiation

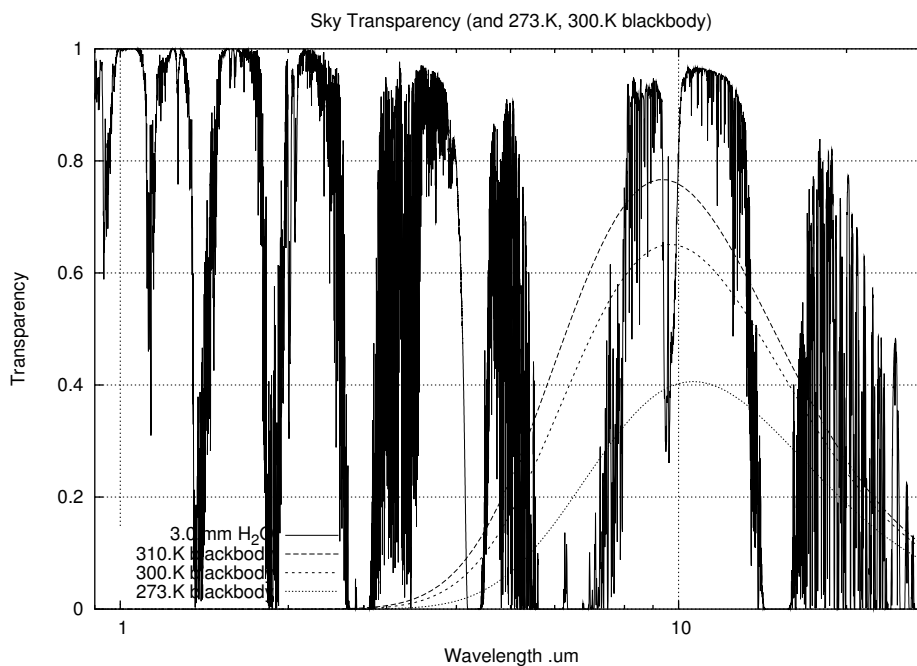
What is the cooling power of blackbody radiation? Radiating from a black body at temperature T into a hemispheric vacuum at temperature T_0 :

$$w_{bb} = (T^4 - T_0^4) \cdot 5.6 \times 10^{-8} \frac{\text{W}}{\text{m}^2 \cdot \text{K}^4} \approx 454 \text{ W} \cdot \text{m}^{-2} \quad \text{at } T = 300 \text{ K} \quad \text{and} \quad T_0 = 3 \text{ K}$$

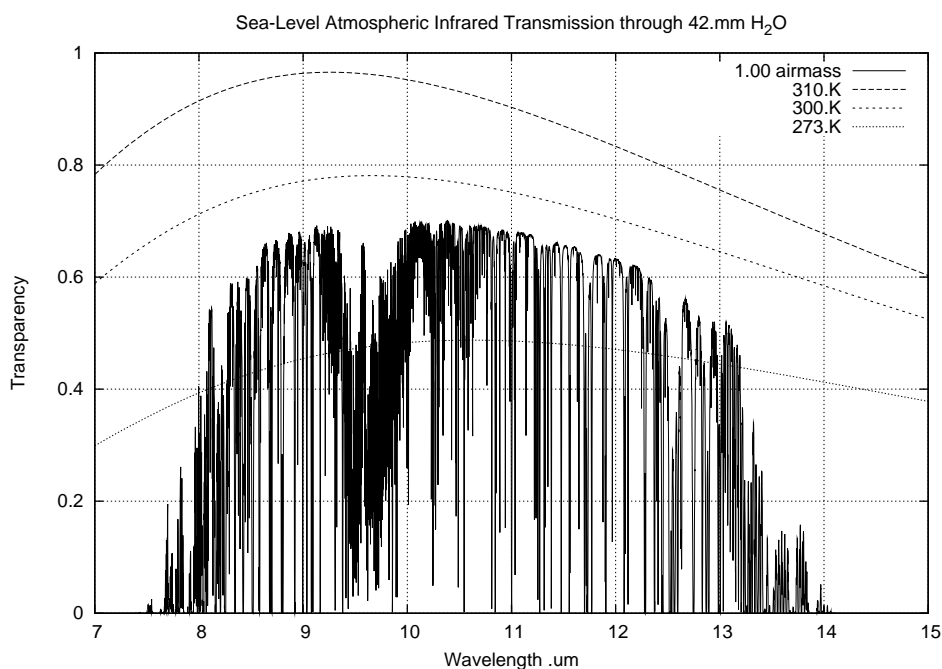
Less than half of this can be achieved due to the infrared absorption by earth’s atmosphere. But significant cooling can be achieved by radiating from the earth’s surface. Natural radiative cooling is manifest as precipitous drops in temperature on nights when the atmosphere is very dry.

Atmospheric Transmittance

The earth's atmosphere absorbs and scatters radiation over much of the infrared band. The Gemini Observatory citing Lord [23] gives atmospheric transmittance spectra from $0.9 \mu\text{m} - 5.6 \mu\text{m}$ and $6 \mu\text{m} - 28 \mu\text{m}$ for low levels of humidity above Mauna Kea.¹



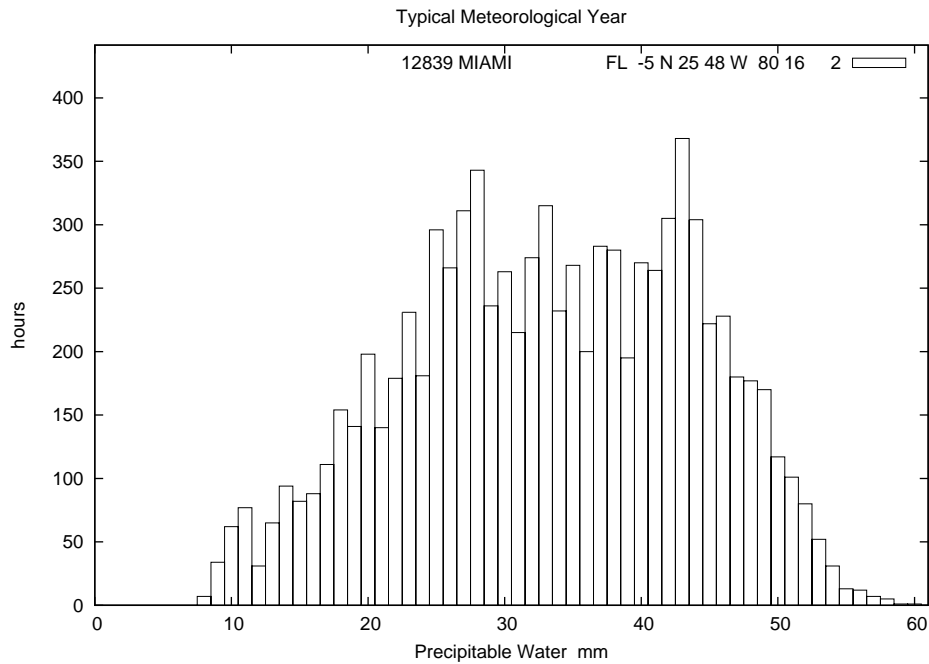
Henry Roe [personal communication] has calculated infrared transmittance data for 37°C saturation humidity at sea-level. Of particular interest is the $8 \mu\text{m} - 13 \mu\text{m}$ infrared “window” encompassing the peaks of blackbody emission radiating from bodies between 0°C and 37°C .



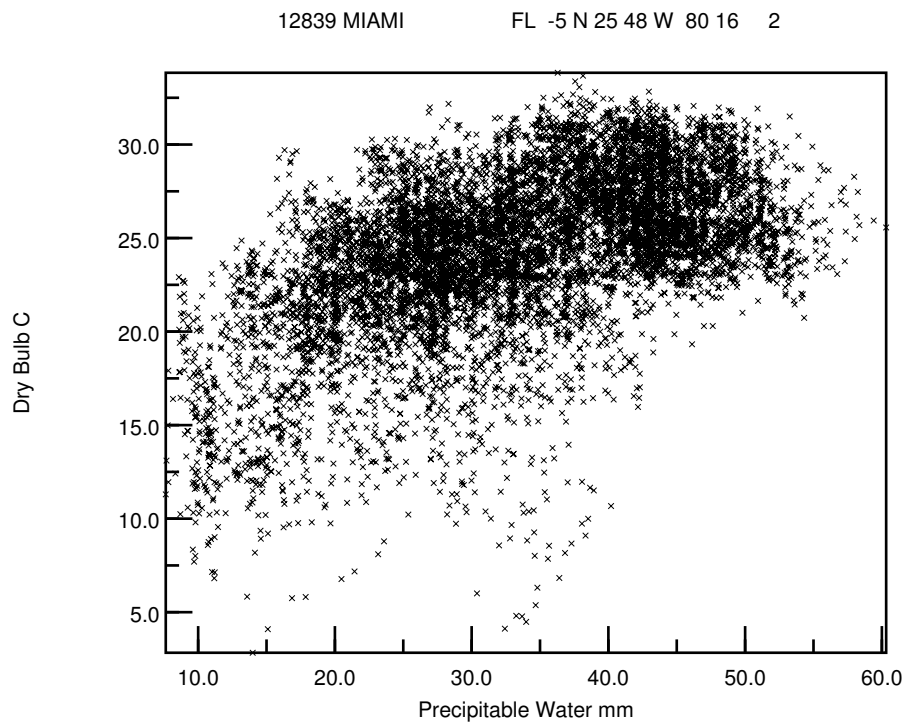
¹ <http://www.gemini.edu/sciops/ObsProcess/obsConstraints/ocTransSpectra.html>

Precipitable Moisture

Precipitable moisture is the depth (in mm) of liquid were all the moisture in a vertical column of atmosphere condensed. A histogram of the hourly precipitable moisture in Miami Florida's typical meteorological year shows peaks at 30 mm and 45 mm.



A scatter-plot of temperature versus precipitable moisture shows that the highest moisture readings occur around 26 °C; while no readings approach 37 °C (310 K).



Airmass

A horizontal plate sees 180° degrees of sky. Transparency is reduced when looking through a larger *airmass*. Limiting the view of the plate to 60° from zenith gives an averaged visible airmass of 1.333. G_C , the ratio of the radiant flux to the hemispherical flux is 0.75 at 60°.

Airmass is not the only reason to limit this angle. Hills, vegetation, and buildings within view of the plate will emit thermal radiation which it could absorb. The daily solar warming of these objects will raise their temperatures above ambient and result in a net transfer of heat into the emitter. So a radiating plate should be deployed by placement on a horizontal roof and spaced from substantial projections so that they are below the plate's cone of view.

The blackbody spectral power density at wavelength λ and temperature T is:

$$M(\lambda, T) = \alpha \lambda^{-5} \left(e^{\beta/\lambda T} - 1 \right)^{-1}$$

The blackbody efficiency $G_B \approx 0.93$, the glazing's infrared transparency $G_F \approx 0.8$, and G_C restrict both incoming and outgoing radiation. The outgoing thermal radiation, $M(\lambda, T)$, is offset by thermal emissions of the atmosphere, $M(\lambda, T_A) \cdot (1 - (A_1(\lambda))^a)$, where a is airmass and $A_1(\lambda)$ the atmospheric transmittance at zenith (airmass of 1). Integrating the radiation balance over wavelength gives the net radiated power density:

$$G_B G_F G_C \int_{\lambda_L}^{\lambda_U} M(\lambda, T) - M(\lambda, T_A) \cdot (1 - (A_1(\lambda))^a) d\lambda$$

$\lambda_L - \lambda_U$	T_A	H ₂ O	$T = 310$ K	$T = 300$ K	$T = 273$ K
1 $\mu\text{m} - 28 \mu\text{m}$	300 K	1 mm	135 W · m ⁻²	106 W · m ⁻²	42 W · m ⁻²
8 $\mu\text{m} - 13 \mu\text{m}$	300 K	1 mm	83 W · m ⁻²	69 W · m ⁻²	39 W · m ⁻²
1 $\mu\text{m} - 28 \mu\text{m}$	300 K	5 mm	110 W · m ⁻²	81 W · m ⁻²	16 W · m ⁻²
8 $\mu\text{m} - 13 \mu\text{m}$	300 K	5 mm	77 W · m ⁻²	63 W · m ⁻²	33 W · m ⁻²
1 $\mu\text{m} - 28 \mu\text{m}$	300 K	42 mm	65 W · m ⁻²	36 W · m ⁻²	-29 W · m ⁻²
8 $\mu\text{m} - 13 \mu\text{m}$	300 K	42 mm	47 W · m ⁻²	33 W · m ⁻²	3 W · m ⁻²
1 $\mu\text{m} - 28 \mu\text{m}$	310 K	42 mm	42 W · m ⁻²	13 W · m ⁻²	-52 W · m ⁻²
8 $\mu\text{m} - 13 \mu\text{m}$	310 K	42 mm	39 W · m ⁻²	25 W · m ⁻²	-5 W · m ⁻²

The transparency data does not distinguish between atmospheric absorption and scattering. This calculation assumes that all radiation not transmitted is absorbed; and that all absorption is matched by proportional blackbody emission. It also assumes that the atmospheric blackbody emission is at the ground level ambient temperature (300 K or 310 K).

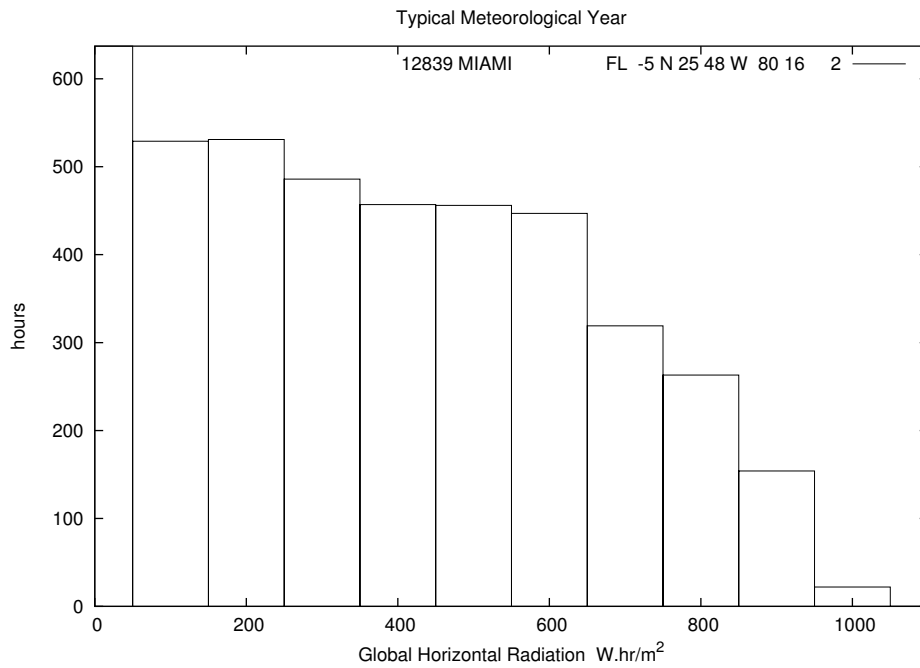
Although the top half of the chart has high cooling rates, the low humidities of the 4205 meter summit of Mauna Kea [21], above 40 percent of the Earth's atmosphere, is not a location typical of the millions of buildings which might benefit from cooling. But the bottom half of the chart shows some cooling activity even in tropical saturation humidity at 37 °C.

In "Passive Cooling" [12] M. Martin writes "A blackbody emitter provides the greatest cooling power when the radiator is at or slightly below the ambient air temperature. The advantage of using a selective radiator is that it is capable of attaining a much lower temperature (the stagnation temperature) than a blackbody under clear sky conditions."

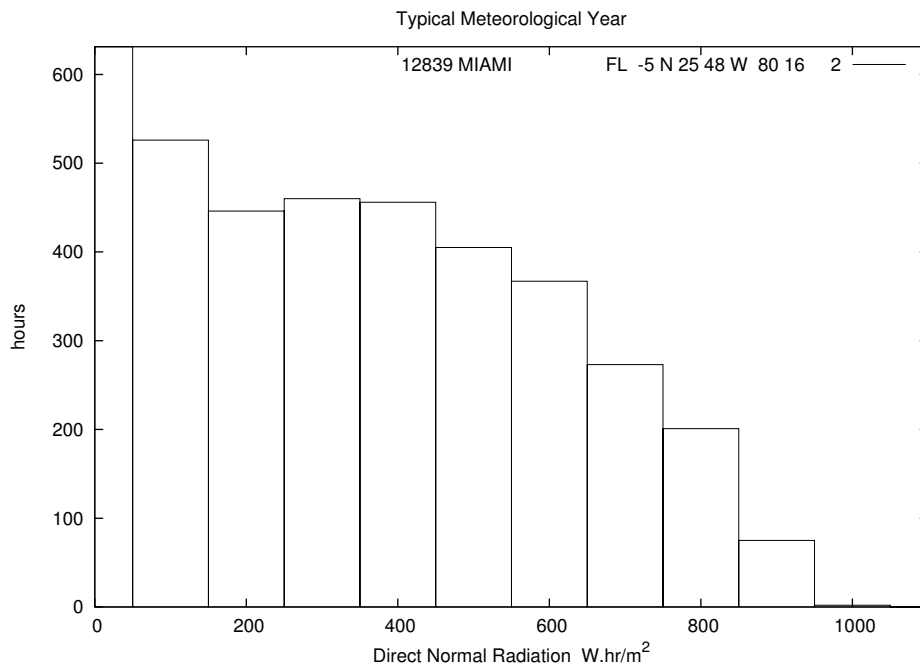
The rows in the chart with a wavelength range 8 $\mu\text{m} - 13 \mu\text{m}$ simulate a perfect ("brick wall") selective emitter. The chart shows selective emitters have less cooling power than non-selective emitters for rooms at or above ambient temperature; consistent with Martin's description. For cooling low-technology tropical buildings, the selective emitter "advantage" is actually a disadvantage. With selective emitters the daily temperatures swings will be amplified, making dwelling interiors uncomfortably cold before dawn.

Selective emitters are the focus of most of the radiative cooling patents; but selective emitters are suboptimal for cooling tropical buildings. Non-selective emitters will cool hot interiors faster.

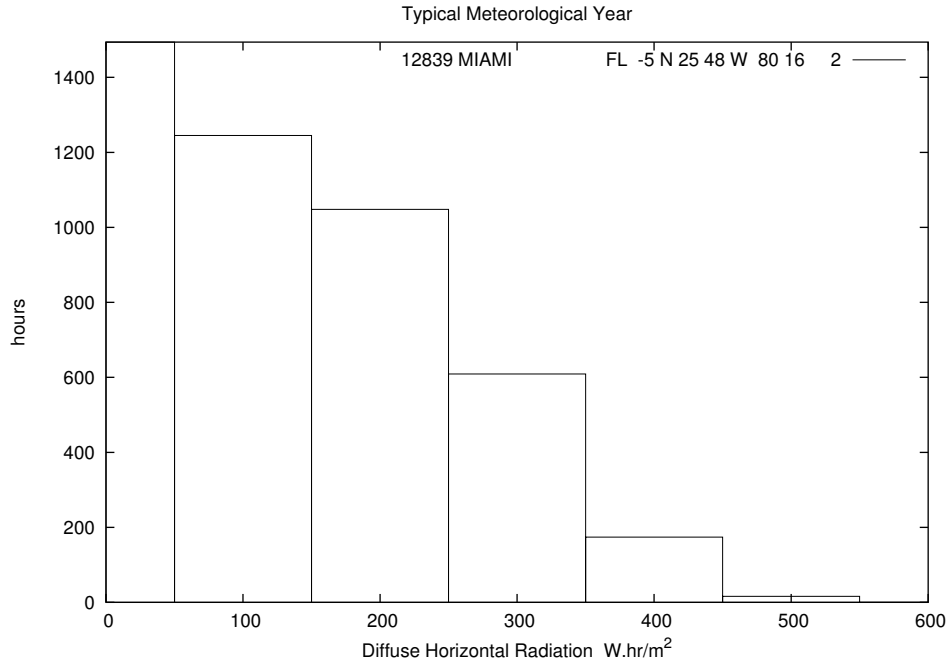
Shedding Light



A histogram of the hourly radiation impinging on 1 m² in Miami Florida's typical meteorological year shows there are thousands of hours when the incoming radiance greatly exceeds the cooling available from blackbody radiation.



Comparing the total radiation with the direct solar radiation shows that diffuse radiation must be a significant contributor on the brightest days.



Merely shielding the cooling radiator from direct sunlight would leave 1800 hours per year when the cooling panel would receive more than 200 W/m².

What about wavelength selectivity?

- 90 % of the sun's radiance is at wavelengths shorter than 1.7 μm.
- 99 % of the sun's radiance is at wavelengths shorter than 4 μm.
- 99.9 % of the sun's radiance is at wavelengths shorter than 9 μm.

- 99.7 % of a 300 K blackbody's radiance is at wavelengths longer than 4 μm.
- 99 % of a 300 K blackbody's radiance is at wavelengths longer than 4.8 μm.
- 90 % of a 300 K blackbody's radiance is at wavelengths longer than 7.3 μm.

A *cold mirror* which reflected waves shorter than 4 μm and transmitted waves longer than 7 μm would allow the radiator to simply face upward through the cold mirror.

Emitters and Concentrators

The Second Law of thermodynamics dictates that the blackbody flux through an aperture can be no greater than that produced by a blackbody at the same temperature having that aperture as its surface.² Thus, blackbody radiation cannot be concentrated by any arrangement of mirrors. The rate of cooling is limited by the blackbody emitter aperture.

With the low efficiency of radiating through humid air, it will be necessary to cover most of the roof area with radiators. For piped fluids, this would be prohibitively expensive. Replacing the roof with radiative panels seems the only strategy which can come in at low enough cost for widespread deployment.

Many radiative cooling schemes employ selective emitters. But in the tropics, the solar heat absorbed a selective emitter will often overwhelm the radiative cooling available. In high solar radiance daylight, roofing which rejects more than 90 % of solar radiation would gain less heat than selective radiators which reject only 80 %; and there are a variety of *cool roof* products designed to reflect solar irradiance. In any case, practical radiative roof panels must reject heat from both direct and indirect solar radiation.

Room-temperature blackbody emitters are common. In some cases, putting an infrared emitter in roof panels isn't necessary; objects and floor can radiate through infrared-transparent roof panels.

² Otherwise, there would be net energy transfer between two blackbodies at the same temperature, which the Second Law forbids.

Prior Work

US patent 3,043,112 issued Jul. 10, 1962 to A. K. Head describes a “Method and means for producing refrigeration by selective radiation” [1]. A selective emitter deposited on a reflective metal heat exchanger is covered by an infrared-transparent layer to “*prevent conductive and convective transfer of ambient heat to the selective absorber*”. The only material mentioned for the insulating layer is polyethylene. Head also suggests that a thin layer of “*germanium or silicon; which is opaque to radiation outside the range of 8 to 13 microns, on the outer face of the insulating region further limits heating by solar radiation.*” This hints at the use of a light absorbing layer in the patent by Silvestrini et al. [3], but does not presage the elimination of the selective emitter by Silvestrini; nor the light-transparent emitter of the present invention; nor the specular solar shield of the present invention. Both germanium and silicon are infrared transparent in films less than 100 nm thick. Both have bandgaps too high for effective solar rejection.

Head’s suggestion of a vertical sunshade for his horizontal emitter is unworkable in the tropics, where the sun is at zenith twice per year; and would require the sunshade to be impractically large because of the high sun angles in the tropics. Vertical sunshades provide practically no ultraviolet protection on cloudy days, which is needed because ultraviolet radiation degrades polyethylene.

For application to cooling a house, Head shows a baffle below the heat exchanger and suggests: “*As the source of cold is above the rooms to be cooled, suitable ducting gives automatic circulation of air.*” The present invention is simpler. It has the emitter in the ceiling; enabling radiative, convective, and conductive transfer of heat to the emitter. Elimination of the baffles and ducting improves the overall efficiency of the cooling process.

US patent 3,310,102 issued Mar. 21, 1967 to F. Trombe describes “Devices for Lowering the Temperature of a Body by Heat Radiation Therefrom” [2]. It uses transparent polyethylene as the window material and polyvinyl chloride or metal oxides as selective radiators.

All his devices are described as pointing north and have reflectors shielding the radiator from direct sunlight. This scheme will be ineffective on cloudy days. And it would require the devices to be aimed horizontally in the tropics, reducing their cooling power by a factor of 3 relative to horizontal emitters, a futile level.

Trombe’s patent shows imagining and non-imagining concentrators much larger than their blackbody emitters. The second law of thermodynamics limits their cooling power to that of the actual emitters. Such large structures will not be economical for the small amount of cooling they would deliver.

Trombe’s nested radiators would surpass the cooling power of a single radiator only if thermal conduction was the limiting factor for cooling. In the vast majority of sites and seasons potentially benefiting from cooling, radiant flux from the sky limits temperature drops. Trombe’s December measurements at Montlouis, Pyrenees-Orientales, France on clear days at temperatures hovering near freezing should not be extrapolated to sea-level saturation humidity in the tropics.

Granqvist and Hjortsberg [10] give a thorough analysis of radiation balance and their selective emitters on reflective aluminum. Putting all the wavelength selectivity in the emitter has the disadvantages:

- Solar heating is part of the load which the emitter must radiate.
- Placing the selective emitter on reflective aluminum does not allow solar lighting through the panel.
- Selective emitters have less cooling power than non-selective emitters when cooling warm buildings.

US patent 4,586,350 issued May 1986 to Berdahl describes “Selective radiative cooling with MgO and/or LiF layers” [4], another selective emitter on a reflective metal substrate. Selective emitters do not perform as well as non-selective emitters for cooling tropical buildings.

Berdahl writes “*A need has existed in the art for materials not in the form of single crystals which can be effectively utilized in selective radiation cooling systems, and particularly such materials that are reflective in the 13-40 micron wavelength range.*”

He accomplishes this with millimeter thick slabs of ceramic MgO or LiF. He reports a *stagnation temperature* of 25 degrees below ambient versus 22 degrees below ambient for a blackbody radiator. Lower stagnation temperature, which comes at the price of lower cooling power for warm interiors, is a disadvantage when cooling tropical buildings.

The present invention differs in that it uses sheets of inexpensive materials like glass or plastics as non-selective infrared radiators which are also transparent to visible light.

About solar shields Berdahl states: “*If the selective radiative cooling material is to be utilized in direct sunlight, the infrared transmitting cover or shield should be opaque in the solar spectrum of 0.3 to 3 microns. The previously-referenced patent to Silvestrini et al gives information for the fabrication of such shields.*”

US patent 4,624,113 issued Nov. 1986 to Hull, “Passive-solar directional-radiating cooling system” [5], combines non-imaging optical concentrators with selective emitters. Selective emitters do not perform as well as non-selective emitters for cooling tropical buildings. As established earlier, the optical concentrators do not improve the cooling power of its small radiators. Its optical concentrators would need to be aimed horizontally in order to avoid direct sunlight in the tropics, reducing its effectiveness below useful levels. On cloudy days, solar heating is part of the load which the emitter must radiate.

US patent 5,405,680 issued Apr. 1995 to Chang et al.[6] describes “Selective emissivity coatings for interior temperature reduction of an enclosure”. Selective emitters produce less cooling than the combination of blackbody emitters with solar screens, which are better suited to cooling tropical buildings.

The reflectivity graphs in the patent show poor performance for its preferred embodiment coating, reflecting more than 50 %, and thus transmitting less than 50 %, of the 8 μm to 13 μm infrared band.

In “Optical Properties and Radiative Cooling Power of White Paints”, Tanemura et al. evaluate white paints (on glass and steel) as broad spectrum IR emitters which reflect solar irradiance [17]. The best has 85 % solar reflectance; while all have close to 93 % IR emittance. They attribute the IR emittance to the paint binders being acrylic or urethane. Even with these high numbers, the combination does not cool during summer days in Nagoya Japan; this supports the need to separate the solar screen from the blackbody emitter.

US patent 4,323,619 issued Apr. 1982 to Silvestrini et al.[3] teaches that high-density polyethylene (HDPE) is 70 % transparent from 8 μm to 13 μm while loaded with enough white pigment to achieve 70 % solar reflectance by scattering. They bond black HDPE film to the back of white HDPE which absorbs the sunlight which has penetrated through the white layer. The carbon black particles are smaller than 5 μm , apparently radiating poorly at wavelengths longer than 5 μm .

For horizontal panels, this arrangement is significantly better than selective radiators. Selective radiators absorb and must radiate the heat from sunlight they don’t reflect. The Silvestrini et al.[3] screen absorbs the residual light, but does not radiate it. Instead, the heat absorbed from sunlight will be cooled by convection from the top surface. The airspace between the screen and the radiating objects thermally isolates them.

The solar transmittance reported for these HDPE sheets ranged from 10 % to 1 %, depending on the thickness and pigment concentrations.

While a straightforward extension of this patent might be to replace the white pigment with similar size metal particles, it would still be light scattering. The present invention differs from the solar screen in that solar radiation is specularly reflected from its top surface. This has the advantages:

- A higher proportion of solar radiation is reflected.
- Less solar radiation need be absorbed by the reflector sheet, keeping it cooler than a diffusing sheet.
- Very thin sheets can be coated and used; increasing the portion of blackbody infrared radiation which it transmits.
- Because little ultraviolet radiation penetrates the reflective coating, it better protects the sheet from degradation caused by ultraviolet light.

In “TiO₂ Nanocrystalline Pigmented Polyethylene Foils for Radiative Cooling Applications: Synthesis and Characterization” [11], Mastai et al. give spectral properties of HDPE loaded with several sizes of TiO₂ crystals, finding that smaller crystals improve the Silvestrini et al.[3] screen.

In “Passive Cooling” [12] M. Martin gives a good overview of radiative techniques and tradeoffs, and practical details. One approach coating polyethylene with tellurium to harden it to the effects of sunlight and weather attributed to Golli and Grenier (1981) is discussed in the next section. Martin writes: “*Further efforts should be directed at increasing the infrared transmissivity of polyethylene, which exhibits a continuum type of background emissivity in the spectral range of the atmospheric window.*”

No practical film with higher IR transparency than HDPE has been reported. Minimizing the IR loss means using the thinnest film possible. But thinness limits the amount of white and black pigments the HDPE can hold. The highest solar reflectivity Silvestrini et al.[3] report is 72 % for a 100 μm thick film; the highest Mastai et al.[11] report is 76 %, also for a 100 μm thick film. HDPE film is available as thin as 6 μm .

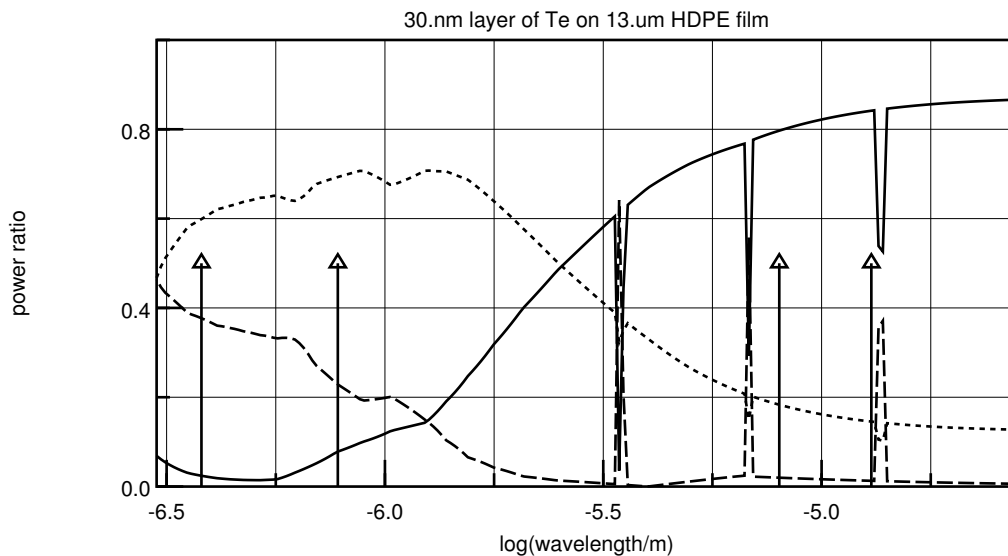
Wavelength Selective Glazing

The genius of Silvestrini et al.[3] was to separate the solar screening component from the blackbody emitter and make that screen nonemitting in the infrared. Thus the solar screen need not be a perfect reflector; it can absorb solar radiation which it does not reflect. But it should be mostly reflective because of Martin's[12] caution: "... polyethylene, which exhibits a continuum type of background emissivity in the spectral range of the atmospheric window." For daytime cooling in the tropics, the separation of the solar screen from the blackbody emitter is crucial.

Solar screen development has previously focused on the scattering properties of white crystals in polyethylene sheet ([3][11]); and the use of semiconductors or semimetals as the solar reflecting layer ([1][6][12][15]). Reflection by scattering requires glazing thickness many times larger than is desirable for maximum infrared transmittance. Also, embedded particles give little protection from HDPE degradation by ultraviolet light.

An exterior layer of semiconductor (or semimetal) can be coated onto a thin sheet of HDPE. The semiconductor is largely transparent to wavelengths whose energies are below the material's bandgap energy. Unfortunately, photons with energy above the bandgap are absorbed and re-radiated, not reflected. Compounding this problem is that photon energy in excess of the bandgap energy is absorbed as heat.

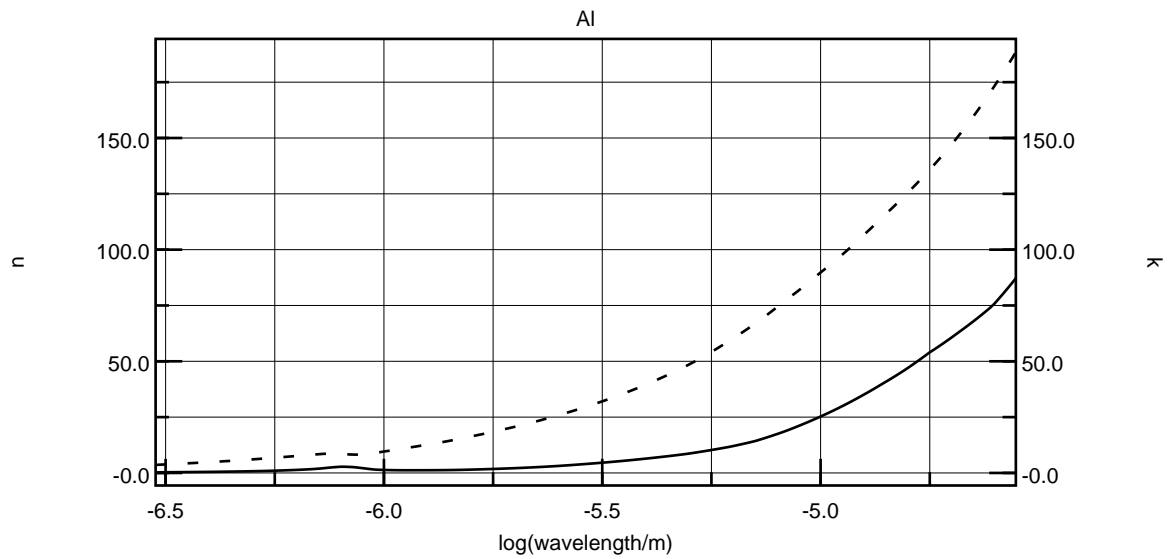
Silicon and Germanium (suggested by Head[1]) have bandgaps too high for this application. Martin[12] reports work by Golli and Grenier (1981) coating 13 μm HDPE with tellurium, whose bandgap is lower. The transmittance spectrum from the book is promising. Calculations show a 30 nm layer of tellurium absorbs 25 % and transmits 9 % of solar irradiance, which is comparable to the solar screen of Silvestrini et al.[3]. Exposing the toxic metal to rain and wind could be problematical.



The University of Reading Infrared Multilayer Laboratory's "Long-Wavelength Pass Filter 2QV" has 92.5 % peak transmittance and cuts from 80 % to 5 % transmittance between 4.548 μm and 4.332 μm [30]. At a cost of 175 GBP, this 10.9 mm diameter by 1.1 mm thick germanium crystal is not practical for cooling; but it demonstrates that coated infrared-transparent materials can be fabricated with ample selectivity.

These sharp dichroic filters are composed of dozens of *dielectric* (electrically insulating) layers deposited on a germanium wafer. Both crystalline germanium and multiple deposition processes are impractically expensive for the large areas radiative cooling requires.

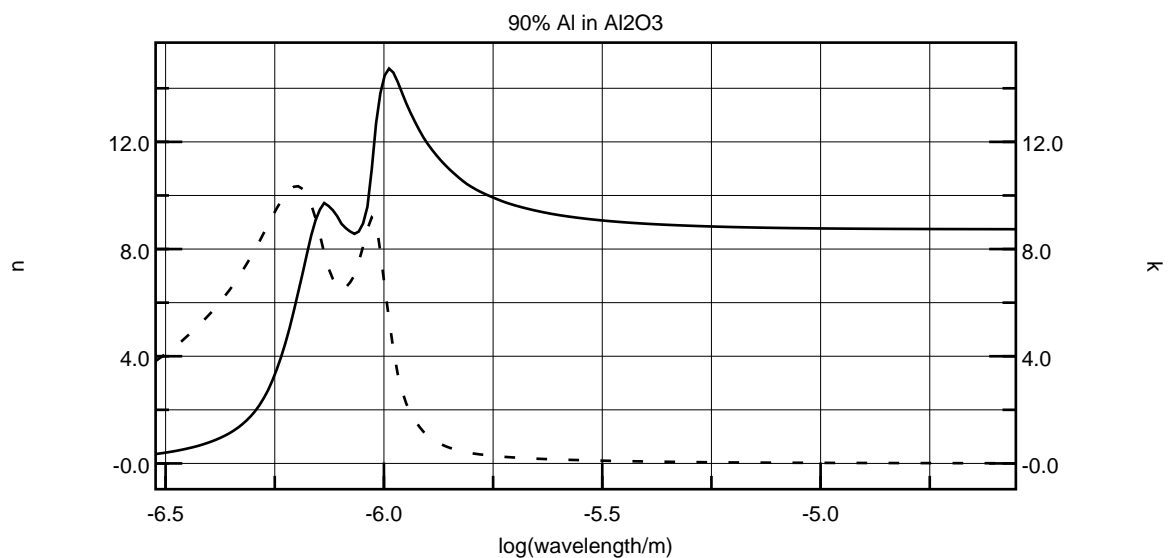
Materials having higher permittivities (and thus higher refractive indexes) are capable of implementing selective filters with fewer layers. Electrically conductive metal layers have very high refractive indexes, but absorb significant portions of incident radiation in the transition band between reflection and transmittance.



The refractive index's exponential increase with wavelength makes an electrically conductive metallic layer highly reflective at long wavelengths; just the opposite of the desired cold mirror! US patent 4,337,990 issued 1982 to Fan and Bachner [7] is a hot mirror formed by a contiguous silver film.

In addition to these problems, depositing thin contiguous metallic layers is difficult and requires rigorous process controls. Both sputtering and evaporative deposition of metals tends to deposit granular thin films [27].

The investigations of J. C. Maxwell Garnett and H. Schopper into the optical properties of small spherical metal particles embedded in a dielectric medium lead to a formula (given in Appendix A) for the effective refractive index [27]. Their analysis applies only when granule sizes are smaller than the shortest wavelengths of light being considered, 300 nm in our case.

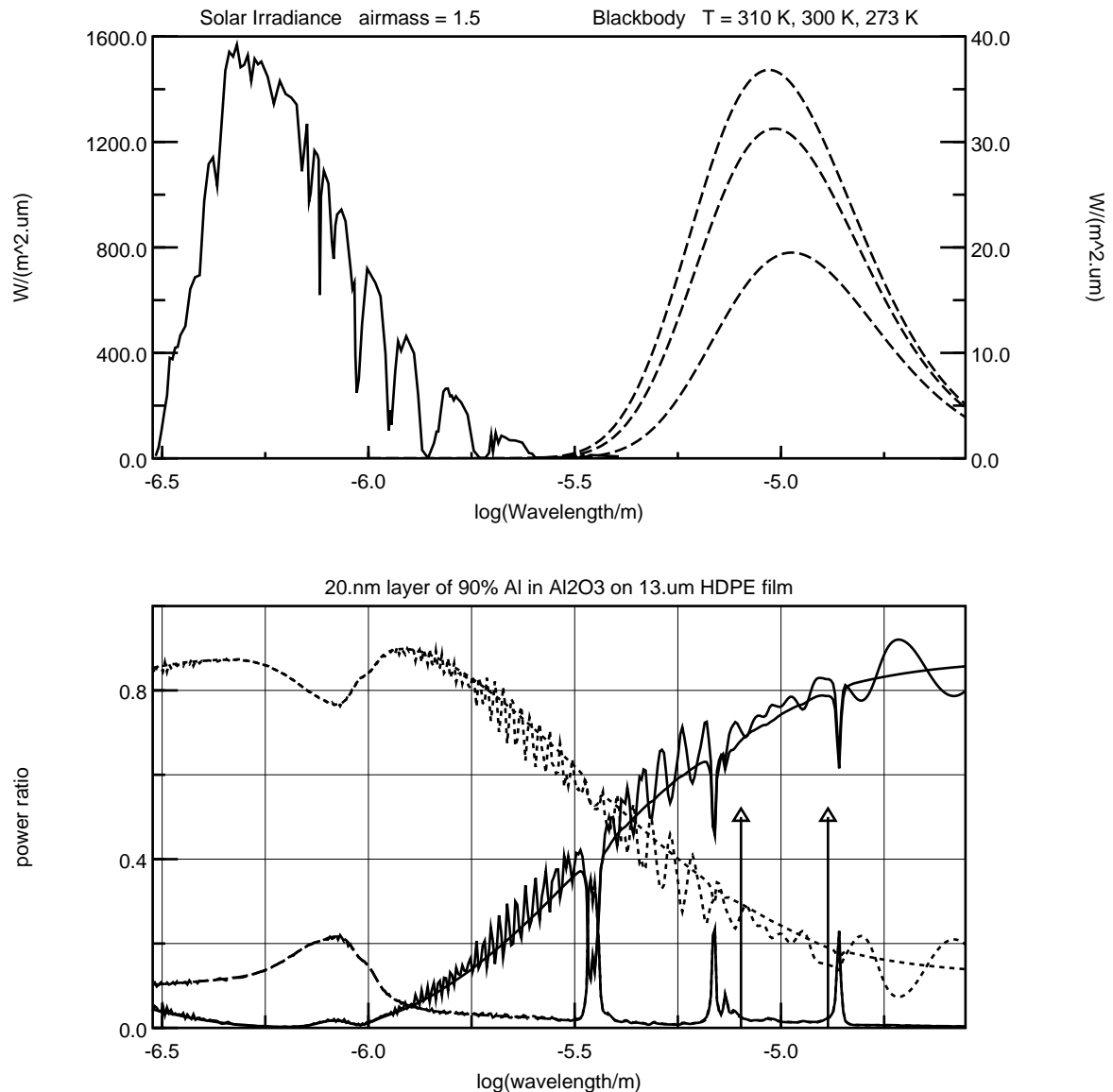


The curves for 90 % granular aluminum embedded in aluminum oxide show a level refractive index and low loss through most of the range of interest. A granular aluminum layer thus acts as a dielectric having an index of refraction of 8.8. Reflections from this layer will be specular, quite unlike a layer of micron diameter TiO_2 or aluminum granules, which would diffusely scatter visible light.

A single 20 nm thick layer of this material gives the desired short wavelength reflectivity and long

wavelength transmittance. According to Alwitt [36], aluminum forms an oxide layer 2 to 3 nm thick. Granules 140 nm in diameter would have the desired volume ratio of 90 %. Sputtering aluminum onto HDPE can produce such granules.

This pair of charts shows the solar spectral irradiance, the blackbody spectral radiance, and the calculated transmittance, reflection, and absorption of the granular aluminum layer on a 13 μm thick sheet of HDPE.



The solid curve is transmittance; dotted is reflection; and dashed is the absorption of radiation from the top surface. The markers delimit the infrared window from 8 μm to 13 μm . The absorption bump at 0.75 μm is from the bulk properties of aluminum. The pairs of absorption lines at 3.45 μm , 6.75 μm , and 13.6 μm are due to C-H and C-C bonds in the HDPE.³ Their depth and the long wavelength absorption are modeled to match the HDPE transmittance curve in reference [10].

Integrating the product of the solar irradiance with the absorption and transmittance curves finds that 13 % of solar irradiance is absorbed; and 3 % is transmitted.⁴

³ <http://www.chem.arizona.edu/courses/chem245/polyeth.html>

⁴ Increasing the HDPE thickness to 100 μm reduces the 11.5 μm transmittance from 80 % to 75 %.

Optics

A function of vertical side walls is to limit the recessed plate's cone of view. For infrared radiation, those side walls must be either reflective or absorbing (and emissive). Absorbing side walls would absorb low-angle rays which are outside of the desired cone. So side walls must be reflective.

Flat vertical walls would reflect low-angle rays between them until they passed over the top of a wall, not limiting the view at all. The curved reflectors of patents [2] and [5] can restrict the aperture to a cone; but these reflecting walls protrude far beyond the extent of the emitter. In addition to presenting high wind loads, these reflecting walls prevent radiators from abutting, reducing the utilization of roof area. As established earlier, no configuration of mirrors can concentrate cooling power from a small emitter.

The only recourse is to have the side walls return infrared radiation to the direction whence it came. Doing so adds no heat load to the emitter. Right angle corner reflectors behave this way. In order that they not be cumbersome in size, multiple small corner reflectors can be formed by corrugating long sheets of reflective metal or metalized plastic, 14.

If the span of the box is so large relative to its height that it absorbs low angle rays, then corrugated corner reflectors, 34, can be spaced across its span to form narrower radiation pyramids.

The thermal conductivity of elements 14 might limit the temperature difference attainable between the glazing 16 and the base 11. But with the corner reflectors supported by rigid insulating foam 13, they need not contact one another. Self-supporting corrugated elements, 34, can be fabricated with each slat connecting to its neighbors at only a few points, thereby increasing their vertical thermal resistance.

The net power flow out of the emitter is:

$$P(T_B, T_0, W) = \int_0^{\pi/2} G_A(\zeta) \int G_F(\lambda, \zeta) G_B(\lambda, \zeta) \cdot \left(M(\lambda, T_B) - S(\lambda, \zeta, T_0, W) \right) d\lambda d\zeta$$

where

T_B is the object (blackbody) temperature;

T_0 is the air temperature at ground level;

W is the precipitable moisture in millimeters;

G_A is the aperture transmittance given in Appendix B;

G_F is the film transmittance;

G_B is the emitter efficiency, here assumed to be a constant 0.93;

M is blackbody emission;

S is the radiation inflow derived in Appendix C;

ζ is the angle from vertical; and

λ is the wavelength.

The aperture's optical transmittance was computed at 91 angles from 0° to 90°. Aperture width to depth ratios of 4, 8 and 16 were simulated. The glazing's optical transmittance was computed at 2000 wavelengths from 0.9 μm to 28 μm and 91 angles from 0° to 90°.

Blackbody radiance from the troposphere was computed at 91 angles integrated over 13804 wavelengths from the lapse rate reduction of temperature with altitude, the density of dry air with altitude, and from the humidity modeled as exponentially decreasing with altitude and normalized to the precipitable moisture.

s/h	ω	T_A	H ₂ O	$T = 310 \text{ K}$	$T = 300 \text{ K}$	$T = 290 \text{ K}$
4.0	76.0°	290 K	25 mm	81 W · m ⁻²	59 W · m ⁻²	39 W · m ⁻²
4.0	76.0°	300 K	35 mm	61 W · m ⁻²	39 W · m ⁻²	19 W · m ⁻²
4.0	76.0°	300 K	45 mm	56 W · m ⁻²	34 W · m ⁻²	14 W · m ⁻²
8.0	82.9°	290 K	25 mm	100 W · m ⁻²	72 W · m ⁻²	47 W · m ⁻²
8.0	82.9°	300 K	35 mm	75 W · m ⁻²	47 W · m ⁻²	22 W · m ⁻²
8.0	82.9°	300 K	45 mm	69 W · m ⁻²	41 W · m ⁻²	16 W · m ⁻²
16.0	86.4°	290 K	25 mm	110 W · m ⁻²	80 W · m ⁻²	52 W · m ⁻²
16.0	86.4°	300 K	35 mm	82 W · m ⁻²	52 W · m ⁻²	24 W · m ⁻²
16.0	86.4°	300 K	45 mm	75 W · m ⁻²	45 W · m ⁻²	17 W · m ⁻²

$h/s = 1/8$ is the case closest to the 60° cone used in the lumped-airmass estimates, both having ratios of aperture flux to hemisphere flux of 0.75. The lumped-airmass estimate of $36 \text{ W} \cdot \text{m}^{-2}$ at 42 mm of precipitable moisture matches the value computed in the isothermal model of Appendix F; and corresponds to the $41 \text{ W} \cdot \text{m}^{-2}$ at 45 mm of precipitable moisture (all with 300 K ambient) shown here. The improvement in cooling power is due to air at elevation emitting blackbody radiation cooler than the ground level ambient temperature. Appendix D visualizes the integration.

Convection and Conduction

When the lower plate is warmer than the glazing, then convection and conduction will aid cooling by transferring heat proportional to the temperature difference. When the lower plate is cooler than the glazing, then conduction will oppose cooling by transferring heat proportional to the temperature difference and inversely proportional to the distance between the plate and glazing.

airspace	upward heat flow	downward heat flow
13 mm	$2.70 \text{ W} \cdot \text{m}^{-2} \cdot \text{K}^{-1}$	$2.27 \text{ W} \cdot \text{m}^{-2} \cdot \text{K}^{-1}$
20 mm	$2.44 \text{ W} \cdot \text{m}^{-2} \cdot \text{K}^{-1}$	$1.61 \text{ W} \cdot \text{m}^{-2} \cdot \text{K}^{-1}$
40 mm	$2.22 \text{ W} \cdot \text{m}^{-2} \cdot \text{K}^{-1}$	$.935 \text{ W} \cdot \text{m}^{-2} \cdot \text{K}^{-1}$
90 mm	$2.00 \text{ W} \cdot \text{m}^{-2} \cdot \text{K}^{-1}$	$.565 \text{ W} \cdot \text{m}^{-2} \cdot \text{K}^{-1}$

A plate which is 10 K cooler than the glazing will have less than $6 \text{ W} \cdot \text{m}^{-2}$ back-flow of heat due to gas conduction if the plate to glazing spacing is 90 mm.

13 % of solar irradiance is absorbed by the granular aluminum coated HDPE glazing. During $500 \text{ W} \cdot \text{m}^{-2}$ incidence, the glazing will absorb $65 \text{ W} \cdot \text{m}^{-2}$. Still air convection will transport about $8 \text{ W} \cdot \text{m}^{-2} \cdot \text{K}^{-1}$ from the top face. Its temperature will rise 8.1 K, causing a $4.6 \text{ W} \cdot \text{m}^{-2}$ reduction in cooling power.

Wind on the glazing increases the convective heat transport, lessening the heat back-flow. At Miami's average daytime wind speed of 5.5 m/s, convection transports $25 \text{ W} \cdot \text{m}^{-2} \cdot \text{K}^{-1}$; and the glazing's temperature will rise only 1.5 K, causing negligible heat back-flow.

Condensation

The latent heat of vaporization of water is $2.26 \times 10^6 \text{ J/kg}$. A 1 m^2 radiator providing 50 W/m^2 of cooling can condense 1 g of water in 45 s; 1 kg in 12.6 hr; or 1.9 kg per day. This amount of condensation is on a par with commercial solar stills from SolAqua [33]:

“Solar still production is a function of solar energy (insolation) and ambient temperature. Production rates in the Southwest U.S. can average about 2 liters per day in the winter to over 6 liters per day during the summer, per square meter.”

10 m^2 of radiators cooling 50 W/m^2 in humid air could produce 19 L of water per day, enough drinking water for six people. Tilting the radiative panels a few degrees and running a drip channel, 30, along the lower edge collects the condensation for use or disposal.

Dynamics

Interior air temperatures can change rapidly. If there is 50 W/m^2 of net cooling, the 2 m column of unsaturated air beneath it cools 1 K every 50 s. Saturated air at 310 K must have .033 g of water vapor condensed from it, requiring an additional 116 J of energy; thus slowing time to cool by 1 K to 52 s.

Performance

The British Thermal Unit is approximately 1055 J of energy. 1 BTU/hr \approx 0.3 W. So a small (4000 BTU/hr) room air conditioner removes 1170 W. To provide this much cooling under conditions of 45 mm precipitable humidity at 27 °C (at sea-level) would require 30 m² of radiating area. But this large area will be offset by there being negligible solar heat absorption by the radiators compared with a non-reflective roof.

Because many of the intended sites for radiative cooling do not have electrical infrastructure, comparison with electrically-powered devices is not the best way to evaluate cooling. We are pursuing radiative cooling to make people comfortable indoors. “Bioclimatic” charts map temperature/humidity domains of human comfort, but are specific for the regions and customs where the trials were performed.

People on average have a metabolic rate of 150 W. This is split between sensible heat and latent heat in the form of water vapor, the ratio depending on the ambient temperature. The load on the radiator to remove these heats is simply 150 W, 3 m² at 50 W/m². Net cooling in excess of this 150 W will reduce the temperature and humidity in the enclosure until it is balanced by heat leakage through the floor and walls.

Conclusion

Inexpensive materials can be fabricated into roof panels providing passive cooling day and night in tropical locations with an unobstructed view of sky.

Deployment of passive cooling radiators in tropical developing regions would improve the health and comfort of the populace without requiring electrical infrastructure; and without contributing to global warming.

Bibliography

- [1] Head, A. K. “Method and means for producing refrigeration by selective radiation”, US patent 3,043,112 issued Jul. 10, 1962.
- [2] Trombe, F. “Devices for Lowering the Temperature of a Body by Heat Radiation Therefrom”, US Patent 3,310,102 issued Mar. 21, 1967.
- [3] Silvestrini, V., Peraldo, M., Monza, E. “Covering Element Screening Off the Solar Radiation for the Applications in the Refrigeration by Radiation”, US Patent 4,323,619 issued Apr. 6, 1982.
- [4] Berdahl, Paul H. “Selective radiative cooling with MgO and/or LiF layers”, US patent 4,586,350 issued May 6, 1986.
- [5] Hull, John R. “Passive-solar directional-radiating cooling system”, US patent 4,624,113 issued Nov. 25, 1986.
- [6] Chang, D., Pollack, S, Shih, I., Jicha, A. “Selective Emissivity Coatings For Interior Temperature Reduction of an Enclosure”, US patent 5,405,680 issued Apr. 11, 1995.
- [7] Fan, J., Bachner, F. “Transparent heat-mirror”, US patent 4,337,990 issued July 6, 1982.
- [10] C. G. Granqvist and A. Hjortsberg. “Radiative cooling to low temperatures: General considerations and application to selectively emitting SiO films”, *Journal of Applied Physics* Vol **52**(6) pp. 4205-4220. June 1981.
- [11] Mastai, Y., Diamant, Y., Aruna, S.T., and Zaban, A. “TiO₂ Nanocrystalline Pigmented Polyethylene Foils for Radiative Cooling Applications: Synthesis and Characterization”, *Langmuir*, **17**, 22, 7118, 7123, 2001, 10.1021/la010370g,
- [12] Martin, M., “Radiative Cooling”, In *Passive Cooling*, edited by Jeffrey Cook. MIT Press, 1989, pp. 138-196.
- [13] “Effects of the Passive Use of Nocturnal Radiative Cooling in Fresh Vegetable Cooling”, National Institute for Rural Engineering, Japan, 2000. <http://www.nkk.affrc.go.jp/eng/topics/reseach/2000/00/nkk/nkk00013.pdf>
- [14] Parker, Danny. “Theoretical Evaluation of the NightCool Nocturnal Radiation Cooling Concept”, Submitted to: U.S. Department of Energy. FSEC-CR-1502-05. April 2005, (Florida Solar Energy Center). <http://www.fsec.ucf.edu/bldg/baihp/pubs/nightcool>

- [15] Tazawa M., Jin P., Tanemura S. “Thin film used to obtain a constant temperature lower than the ambient”,
Thin Solid Films **281-282**, 232-234. 1996.
- [16] Tazawa M., Jin P., Yoshimura K., Miki T. and Tanemura S. “New material design with $V_{1-x}W_xO_2$ film for sky radiator to obtain temperature stability”,
Solar Energy **64**, 37. 1997.
- [17] S. Tanemura, M. Tazawa, P. Jing, T. Miki, K. Yoshimura, K. Igarashi, M. Ohishi, K. Shimono, M. Adachi, “Optical Properties and Radiative Cooling Power of White Paints”,
ISES 1999 Solar World Congress
- [18] Steve Davidson, “SkyCool - extraordinary paint on a hot tin roof.”
ECOS 2004, 12-12. <http://www.publish.csiro.au/paper/EC119p12>
- [20] “Air Mass 1.5 Global Spectrum”,
Key Centre for Photovoltaic Engineering UNSW, 1994.
- [21] The University of Hawaii, “About Mauna Kea Observatories”,
http://www.ifa.hawaii.edu/mko/about_maunakea.htm
- [22] University of Wisconsin Lidar Group, “AERI Microwindow Regions”,
http://lidar.ssec.wisc.edu/papers/dhd_thes/node28.htm
- [23] Lord, Steven D., “A new software tool for computing Earth’s atmospheric transmission of near- and far-infrared radiation”,
NASA Center for AeroSpace Information (CASI) NASA-TM-103957, 1992.
- [24] Pankove, J. I. “Optical Processes in Semiconductors”,
New York: Dover Publication, 1971.
- [25] Horn, Berthold K. P. “The Facts of Light”,
Working Paper 97, MIT Artificial Intelligence Laboratory, 1975.
- [27] Heavens, O. S. “Optical Properties of Thin Solid Films”,
Dover Publications, 1991.
- [28] 1997 ASHRAE Handbook-Fundamentals (SI),
American Society of Heating, Refrigerating and Air-Conditioning Engineers, Inc., Atlanta, US, 1997.
- [29] M. Kenworthy. “Airmass due to the finite radius of the Earth”, 22nd Jan 2002,
http://mmtao.org/mattk/docs/acc_airmass.pdf
- [30] “Long-Wavelength Pass Filters”,
<http://www.cyber.rdg.ac.uk/ISP/infrared/products/catalogue/lwp.htm>,
University of Reading, Infrared Multilayer Laboratory, Reading Berkshire, UK, 2004.
- [31] Jaffer, Aubrey. “FreeSnell Thin-Film Optical Simulator”, Version 1b4, March 2006.
<http://swiss.csail.mit.edu/~jaffer/FreeSnell>
- [32] Bhattacharya, Shaoni. “European heatwave caused 35,000 deaths”,
NewScientist.com 10 October 2003,
<http://www.newscientist.com/channel/earth/climate-change/dn4259>
- [33] “Solar Still Basics”,
<http://www.solaqua.com/solstilbas.html>,
SolAqua, El Paso, Texas.
- [34] Marion, W., Urban K., “User’s Manual for TMY2s, Typical Meteorological Years”,
National Renewable Energy Laboratory, June 1995.
http://rredc.nrel.gov/solar/pubs/tmy2/tmy2_index.html
- [35] Tsilingiris, P. T., “Comparative evaluation of the infrared transmission of polymer films”,
Energy Conversion and Management, Volume 44, Issue 18, November 2003, Pages 2839-2856
- [36] Alwitt, Robert S., “Anodizing”,
Electrochemistry Encyclopedia, Boundary Technologies, Inc., 2002.
<http://electrochem.cwru.edu/ed/encycl/art-a02-anodizing.htm>
- [37] Gail Schiller Brager and Richard de Dear, “A Standard for Natural Ventilation”,
ASHRAE Journal, October 2000
- [38] Bjarne W. Olesen and Gail S. Brager, “A Better Way to Predict Comfort”,
ASHRAE Journal, August 2004

- [40] Reitan, C., “Surface Dew Point and Water Vapor Aloft”,
Journal of Applied Meteorology: Vol. 2, No. 6, pp. 776-779, 1963.
- [41] Smith, W.L., “Note on the Relationship Between Total Precipitable Water and Surface Dew Point”,
Journal of Applied Meteorology: Vol. 5 No. 5, pp 726-727, 1966.
- [42] Viswanadham, Point, “The Relationship between Total Precipitable Water and Surface Dew Point”,
Journal of Applied Meteorology: Vol. 20, No. 1, pp. 3-8, 1981.
- [43] Raymond, William H., “Estimating Moisture Profiles Using a Modified Power Law”,
Journal of Applied Meteorology: Vol. 39, No. 7, pp. 1059-1070, 2000.

Appendix A - Granular Metal Effective Refractive Index

Heavens [27] relates \mathbf{n}_e , the effective refractive index, to \mathbf{n} , the bulk metal refractive index; and q , the volume fraction of spheres in the composite thus:

$$\frac{\mathbf{n}_e^2 - 1}{\mathbf{n}_e^2 + 2} = q \frac{\mathbf{n}^2 - 1}{\mathbf{n}^2 + 2}$$

Solving for \mathbf{n}_e^2 :

$$\mathbf{n}_e^2 = \frac{2 + \mathbf{n}^2 + 2(\mathbf{n}^2 - 1)q}{2 + \mathbf{n}^2 + (1 - \mathbf{n}^2)q}$$

But a refractive index of 1 for the dielectric is usually not the case. Change the dielectric constant of the vacuum to \mathbf{n}_s and rederive:

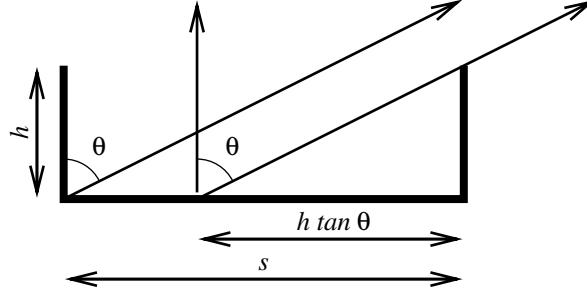
$$\frac{\mathbf{n}_e^2}{\mathbf{n}_s^2} = \frac{\mathbf{n}^2 + 2\mathbf{n}_s^2 + 2(\mathbf{n}^2 - \mathbf{n}_s^2)q}{\mathbf{n}^2 + 2\mathbf{n}_s^2 + (\mathbf{n}_s^2 - \mathbf{n}^2)q}$$

Solving for \mathbf{n}_e :

$$\mathbf{n}_e = \mathbf{n}_s \sqrt{\frac{\mathbf{n}^2 + 2\mathbf{n}_s^2 + 2(\mathbf{n}^2 - \mathbf{n}_s^2)q}{\mathbf{n}^2 + 2\mathbf{n}_s^2 + (\mathbf{n}_s^2 - \mathbf{n}^2)q}}$$

This is the formula used by the *FreeSnell* program [31] for granular films.

Appendix B - Square Aperture



A Lambertian blackbody radiates into the whole hemisphere. The recessed emitter restricts emission to a pyramid centered on the zenith. Given a $s \times s$ plate with a $s \times s$ aperture h directly above it, a ray inclined θ from vertical sees

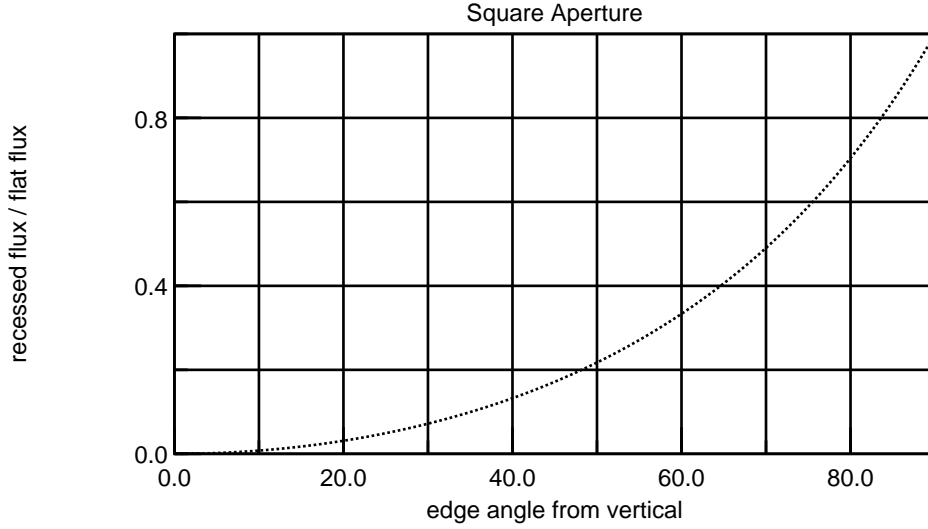
$$1 - \frac{h}{s} \tan \theta$$

of the plate. The largest angle seeing any of the plate is

$$\omega = \arctan \frac{s}{h}, \quad h = \frac{s}{\tan \omega}.$$

For a unit square ($s = 1$) Lambertian radiator, the ratio of recessed flux to flat hemispherical flux is:

$$\int_0^\omega \int_0^\omega \left(1 - \frac{\tan \theta}{\tan \omega}\right) \cos \theta \left(1 - \frac{\tan \phi}{\tan \omega}\right) \cos \phi d\theta d\phi = \left(\sin \omega + \frac{\cos \omega - 1}{\tan \omega}\right)^2$$



But the aperture gain, G_A , needs to be in terms of ζ , the angle from vertical. The unit vector at angle ζ from zenith and azimuth ψ is:

$$\vec{Q} = [\sin \psi \sin \zeta, \cos \psi \sin \zeta, \cos \zeta].$$

The projections of \vec{Q} onto the xz and yz planes do not necessarily have unit length:

$$\begin{aligned} & [\sin \psi \sin \zeta, \cos \zeta], \quad [\cos \psi \sin \zeta, \cos \zeta] \\ \tan \theta &= \sin \psi \tan \zeta, \quad \tan \phi = \cos \psi \tan \zeta \\ \frac{\tan \theta}{\tan \phi} &= \tan \psi, \quad \tan^2 \theta + \tan^2 \phi = \tan^2 \zeta \end{aligned}$$

Let $u = \tan \theta$, $v = \tan \phi$, and $h = 1/\tan \omega$. Then $du = d\theta/\cos^2 \theta$ and $dv = d\phi/\cos^2 \phi$.

$$\int_0^\omega \int_0^\omega \left(1 - \frac{\tan \theta}{\tan \omega}\right) \cos \theta \left(1 - \frac{\tan \phi}{\tan \omega}\right) \cos \phi d\theta d\phi = \int_0^{1/h} \int_0^{1/h} \frac{(1-hu)(1-hv)}{(1+u^2)^{3/2}(1+v^2)^{3/2}} du dv$$

Let $x = \tan \psi$.

$$\begin{aligned} \tan \theta = u &= \frac{x \tan \zeta}{\sqrt{1+x^2}}, \quad \tan \phi = v = \frac{\tan \zeta}{\sqrt{1+x^2}} \\ \frac{u}{v} &= x, \quad u^2 + v^2 = \tan^2 \zeta \end{aligned}$$

$$J(x, z) = \det \begin{pmatrix} \frac{\partial u}{\partial x} & \frac{\partial u}{\partial \zeta} \\ \frac{\partial v}{\partial x} & \frac{\partial v}{\partial \zeta} \end{pmatrix} = \det \begin{pmatrix} \frac{\tan \zeta}{(x^2+1)^{3/2}} & \frac{\sec^2 \zeta x}{(x^2+1)^{1/2}} \\ -\frac{\tan \zeta x}{(x^2+1)^{3/2}} & \frac{\sec^2 \zeta}{(x^2+1)^{1/2}} \end{pmatrix} = \frac{\sec^2 \zeta \tan \zeta}{x^2 + 1}$$

The integrand in terms of h , x , and ζ is:

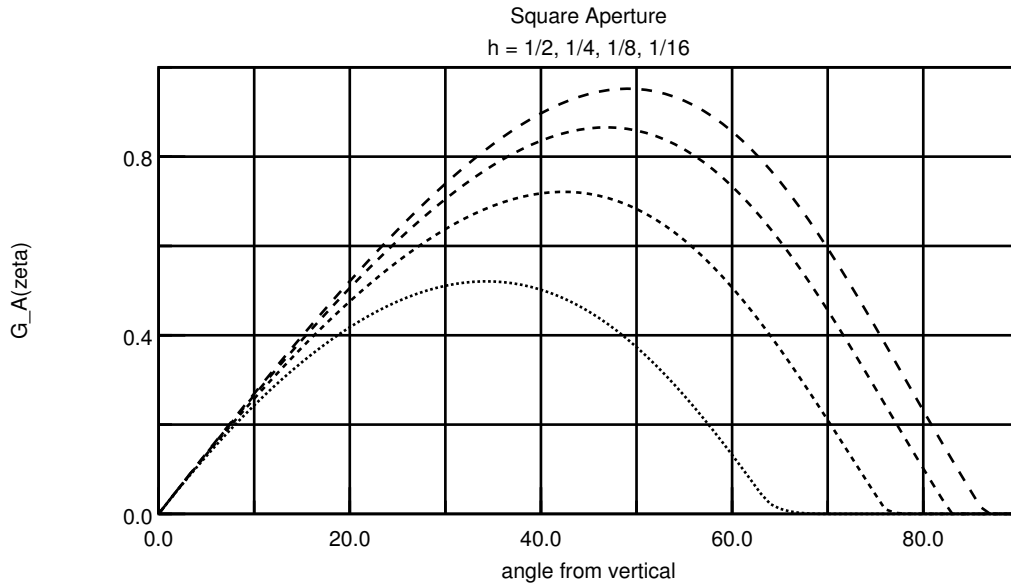
$$I(h, x, \zeta) = \left(1 - \frac{h \tan \zeta}{\sqrt{x^2 + 1}}\right) \left(1 - \frac{hx \tan \zeta}{\sqrt{x^2 + 1}}\right) \left(\frac{\tan^2 \zeta}{x^2 + 1} + 1\right)^{-\frac{3}{2}} \left(\frac{x^2 \tan^2 \zeta}{x^2 + 1} + 1\right)^{-\frac{3}{2}} \frac{\tan \zeta}{(x^2 + 1) \cos^2 \zeta}$$

The integral is then:

$$2 \int_0^\omega \int_0^1 I(h, x, \zeta) dx d\zeta + 2 \int_{\arctan(\sqrt{2} \tan \omega)}^{\arctan(\sqrt{2} \tan \omega)} \int_{\sqrt{h^2 \tan^2 \zeta - 1}}^1 I(h, x, \zeta) dx d\zeta$$

And:

$$G_A(\zeta) = \begin{cases} 2 \int_0^1 I(h, x, \zeta) dx, & \text{if } 0 \leq \zeta \leq \omega; \\ 2 \int_{\sqrt{h^2 \tan^2 \zeta - 1}}^1 I(h, x, \zeta) dx, & \text{if } \omega \leq \zeta \leq \arctan(\sqrt{2} \tan \omega); \\ 0, & \text{otherwise.} \end{cases}$$

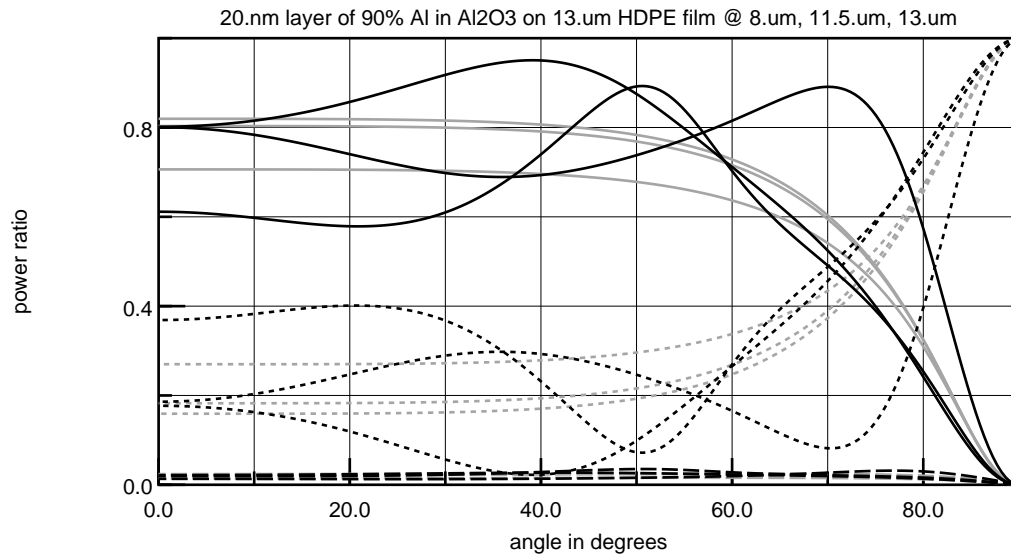


G_A integrated over ζ is the ratio of aperture flux to hemispheric flux. h is the ratio of recess depth to length of the side; and $\omega = \arctan(1/h)$, the largest angle (from vertical) receiving flux from above.

h	ω	$\int G_A(\zeta) d\zeta$	h	ω	$\int G_A(\zeta) d\zeta$
1/2	63.4°	0.38	1/8	82.9°	0.78
1/4	76.0°	0.61	1/16	86.4°	0.89

It is desirable to limit the width of the radiative pyramid because the atmosphere seen at large ζ angles is opaque and emissive with temperature at or above ambient. Depth-to-side ratios between 1/4 and 1/8 look to have a good balance between efficiency and horizontal rejection.

The metalized glazing becomes reflective for nearly horizontal rays. The light gray traces are computed ignoring interference within the HDPE film:



The metalized glazing will help reduce absorption at angles greater than 75° (from vertical) for emitters with $h \leq 1/8$.

Appendix C - Modeling The Troposphere

In the lower atmosphere ($Z = 9$ km), the moist adiabatic lapse rate L averages 6.5 K/km. So the temperature at altitude z is roughly $T_0 - Lz$.

The air pressure P and density r at altitude z are

$$P(z) = P_0 \left(\frac{T_0 - Lz}{T_0} \right)^{g/(LR)} \quad r(z) = \frac{P_0}{R \cdot (T_0 - Lz)} \left(\frac{T_0 - Lz}{T_0} \right)^{g/(LR)} = \frac{P_0}{T_0 R} \left(\frac{T_0 - Lz}{T_0} \right)^{g/(LR)-1}$$

where $R = 287 \text{ m}^2 \cdot \text{s}^{-2} \cdot \text{K}^{-1}$ is the gas constant for air, and g is the gravitational acceleration. $g/(LR) \approx 5.253$. Let $\rho(z, T_0) = r(z, T_0)/\nu$ be the density normalized so that the integral, Q , of ρ over Z at $T_0 = 300$ K is airmass of 1.

$$1 = Q(Z, T_0) = \int_0^Z \rho(z, T_0) dz = \int_0^Z \frac{P_0}{\nu T_0 R} \left(\frac{T_0 - Lz}{T_0} \right)^{g/(LR)-1} dz = \frac{P_0}{\nu g} \cdot \left(1 - \left(\frac{T_0 - LZ}{T_0} \right)^{g/(LR)} \right)$$

$$\nu \approx 7.03 \times 10^3 \text{ g} \cdot \text{m}^{-4}$$

The saturation humidity decreases exponentially with temperature, hence it decreases exponentially with altitude. "Surface Dew Point and Water Vapor Aloft" [40] posits that vapor density (saturated or not) is exponentially decreasing through the troposphere.

Let W be the depth in millimeters of water from a vertical column of atmosphere were its water condensed. Let $w(z, W) = \nu W e^{-\beta z}$ be the precipitable moisture depth (in millimeters) per unit height of a vertical column at altitude z .

$$W = \int_0^Z w(z, W) dz = \int_0^Z \nu W e^{-\beta z} dz = \frac{\nu W}{\beta} (1 - e^{-\beta Z}) \quad \text{where } \beta = 0.44 \text{ km}^{-1}.$$

$$\text{At } Z = 9 \text{ km, } \nu = \frac{\beta}{(1 - e^{-\beta Z})} = 0.449 \text{ km}^{-1}.$$

Let $\tau(z)$ be the transmittance through an atmospheric column to altitude z . The logarithm of transmittance, K , is composed of dry and 1 mm of humidity components:

$$\tau(z) = e^{K(z, \lambda, \zeta, T_0, W)}; \quad K(z, \lambda, \zeta, T_0, W) = \left(\log B(\lambda) Q(z, T_0) + \log H_1(\lambda) \frac{\nu W - w(z, W)}{\beta} \right) \cdot \alpha(\zeta)$$

where $\alpha(\zeta)$ is the airmass at angle ζ from zenith. Two formulas for airmass are [29]:

$$\alpha(\zeta) = \frac{1}{\cos \zeta} \quad \text{and} \quad \alpha(\zeta) = \frac{1}{r} \left(\sqrt{\cos^2 \zeta + 2r + r^2} - \cos \zeta \right) \quad \text{where } r = \frac{8.75}{6378}$$

The choice does not materially effect the results of simulation.

The derivative of transmittance τ with respect to z is:

$$\kappa(z) = \frac{\partial \tau(z, \lambda, \zeta, T_0, W)}{\partial z} = e^{K(z, \lambda, \zeta, T_0, W)} \cdot K'(z, \lambda, \zeta, T_0, W) = \tau(z) \cdot K'(z, \lambda, \zeta, T_0, W)$$

where

$$K'(z, \lambda, \zeta, T_0, W) = \frac{\partial K(z, \lambda, \zeta, T_0, W)}{\partial z} = (\log B(\lambda) \rho(z, T_0) + \log H_1(\lambda) w(z, W)) \cdot \alpha(\zeta)$$

The attenuated emission per unit length at altitude z is $-M(\lambda, T_0 - Lz) \cdot \kappa(z)$. Thus the flow of blackbody radiation from the troposphere into the emitter is:

$$S(\lambda, \zeta, T_0, W) = \int_0^Z -M(\lambda, T_0 - Lz) \cdot \kappa(z) dz$$

The contributions from small z dominate the integral; so linear integration steps have poor numerical conditioning. Let $z = \exp(y)$.

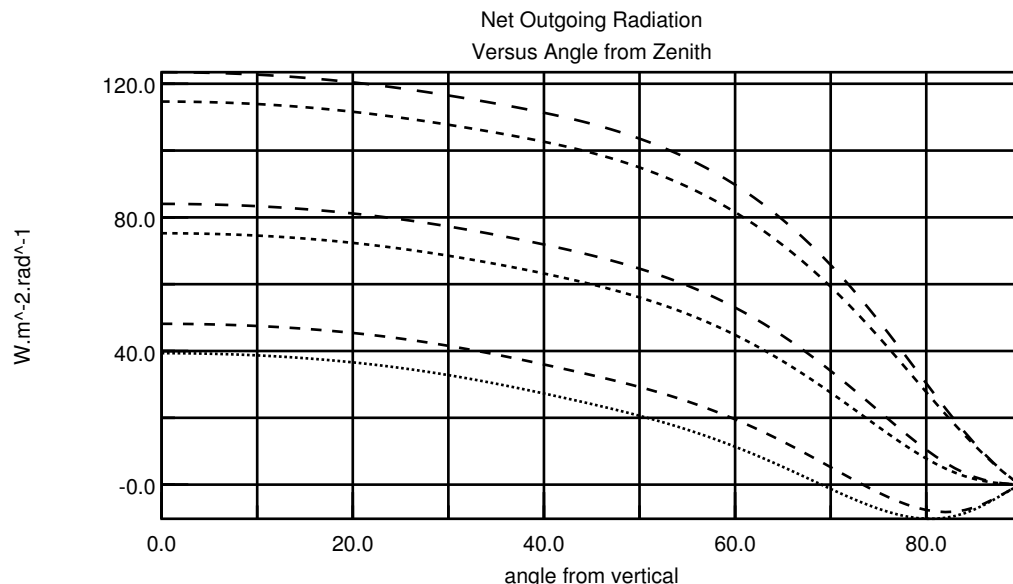
$$S(\lambda, \zeta, T_0, W) = \int_{-\infty}^{\log Z} -M(\lambda, T_0 - L e^y) \cdot \kappa(e^y) e^y dy \approx \int_{-\log Z}^{\log Z} -M(\lambda, T_0 - L e^y) \cdot \kappa(e^y) e^y dy$$

Appendix D - Integrating Over the Sky

The net power flow out of the emitter is:

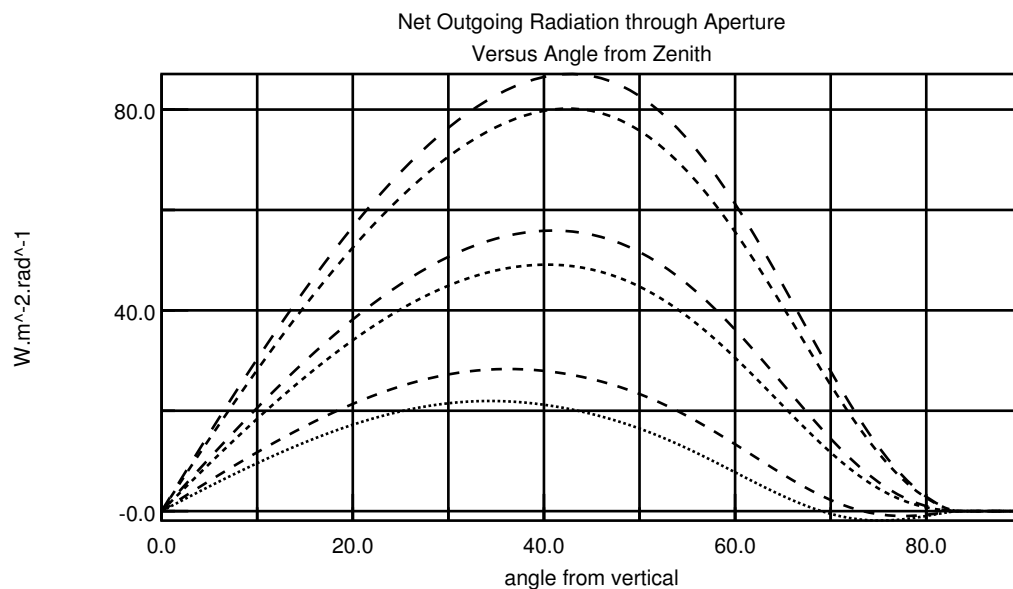
$$P(T_B, T_0, W) = G_B \int_0^{\pi/2} G_A(\zeta) \int G_F(\lambda, \zeta) \cdot (M(\lambda, T_B) - S(\lambda, \zeta, T_0, W)) d\lambda d\zeta$$

The results of the inner integral are plotted below. The traces from top to bottom have precipitable moisture and interior temperature: 35 mm and 310 K; 45 mm and 310 K; 35 mm and 300 K; 45 mm and 300 K; 35 mm and 290 K; and 45 mm and 290 K. The ground-level ambient air temperature for all is 300 K.



When the interior temperature is 290 K, the traces runs negative at high angles because the large airmass blocks visibility of the cooler air at higher elevations.

The outer integral sums the angle-wise product of the net radiative flow and G_A :



Appendix E - Atmospheric Absorption Data

The Gemini Observatory gives atmospheric transmittance spectra for low levels of humidity above Mauna Kea.⁵ These spectra are smoothed down to 13800 values from 1.08×10^6 elements calculated by the ATRAN program [23], a 78 fold reduction.

The mass of the dry air between sea level and the Mauna Kea summit at 4205 m is $Q(4205, 300) = 0.580$. To turn this into airmass 1 data each transmittance value is raised to the reciprocal of 0.580:

$$A^{1/0.580}(\lambda) = A^{1.723}(\lambda)$$

These numbers being raised to powers in the calculation of S makes extrapolation of transmittance of humid atmospheres risky. The 42 mm (of precipitable moisture) Roe data at 1×10^6 wavelengths from $7 \mu\text{m}$ to $15 \mu\text{m}$ was averaged to 1601 values to be used with the Mauna Kea spectra. Spot checks of the averaged values found the wavelength of transitions matched the Mauna Kea data.

The calculation in Appendix C requires that absorption from moisture and that from dry atmosphere be separated. The dry atmosphere transmittance can be extracted from spectra computed for different levels of precipitable moisture. Let $A_W(\lambda)$ be the spectral transmittance value computed for W millimeters of precipitable moisture. $A_3(\lambda)/A_1(\lambda)$ is the transmittance due to 2 mm of water; and $\sqrt{A_3(\lambda)/A_1(\lambda)}$ is the transmittance for 1 mm of water. The dry transmittance is then:

$$A_0(\lambda) = \frac{A_1(\lambda)}{\sqrt{A_3(\lambda)/A_1(\lambda)}} = \sqrt{\frac{A_1(\lambda)}{A_3(\lambda)}}$$

In order to minimize the distortion due to smoothing at high humidities, the absorption of water should be computed using the most humid data available. For the range $0.9 \mu\text{m}$ to $5.6 \mu\text{m}$, that is 3 mm. The Roe data for 42 mm spans the range $7 \mu\text{m}$ to $15 \mu\text{m}$. The rest is 5 mm.

$$A_{\text{H}_2\text{O}}(\lambda) = \left(\frac{A_{42}(\lambda)}{A_0(\lambda)}\right)^{1/42} ; \quad A_{\text{H}_2\text{O}}(\lambda) = \left(\frac{A_5(\lambda)}{A_0(\lambda)}\right)^{1/5}$$

When an $A_1(\lambda)$ transmittance value is 0, $A_0(\lambda)$ and $A_{\text{H}_2\text{O}}(\lambda)$ are set to 0. When the value computed for $A_0(\lambda)$ is greater than 1, $A_0(\lambda)$ is set to 1.

In the range $0.9 \mu\text{m}$ to $5.6 \mu\text{m}$, working from 3.0 mm H₂O and 1.0 mm H₂O Mauna Kea data, there are 206 wavelengths where the value computed for $A_0(\lambda)$ is greater than 1. All but 12 of these are less than 1.001. The 12 outliers ranging from 1.2 to 46 are all at wavelengths greater than $2.5 \mu\text{m}$.

In the range $6 \mu\text{m}$ to $28 \mu\text{m}$, working from 5.0 mm H₂O and 1.0 mm H₂O Mauna Kea data, there are 23 wavelengths where the value computed for $A_0(\lambda)$ is greater than 1. Their values range from 1.01 to 16.6.

In the range $7 \mu\text{m}$ to $15 \mu\text{m}$, working from 42.0 mm H₂O Roe data and 1.0 mm H₂O Mauna Kea data, there are 12 wavelengths where the value computed for $A_{\text{H}_2\text{O}}(\lambda)$ is greater than 1. Their values are between 1 and 1.01 and are at wavelengths from $9.4650 \mu\text{m}$ to $9.6600 \mu\text{m}$.

⁵ <http://www.gemini.edu/sciops/ObsProcess/obsConstraints/ocTransSpectra.html>

Appendix F - Verifying the Tropospheric Model

Running the 60.0° cone with the isothermal tropospheric model yields results within 3 % of the lumped-airmass cooling calculations when the interior is not cooler than ambient. The isothermal rows were run with an effectively zero lapse-rate in the tropospheric model of Appendix C.

The “lapse-rate” rows show significant cooling gains compared to the other rows because some of the air (at elevation) emitting blackbody radiation is cooler than the ground-level ambient temperature.

Troposphere Model	T_A	H ₂ O	$T = 310$ K	$T = 300$ K	$T = 273$ K
lapse-rate	300 K	1 mm	148 W · m ⁻²	120 W · m ⁻²	58 W · m ⁻²
isothermal	300 K	1 mm	135 W · m ⁻²	107 W · m ⁻²	46 W · m ⁻²
lumped	300 K	1 mm	135 W · m ⁻²	106 W · m ⁻²	42 W · m ⁻²
lapse-rate	300 K	5 mm	120 W · m ⁻²	93 W · m ⁻²	31 W · m ⁻²
isothermal	300 K	5 mm	108 W · m ⁻²	81 W · m ⁻²	19 W · m ⁻²
lumped	300 K	5 mm	110 W · m ⁻²	81 W · m ⁻²	16 W · m ⁻²
lapse-rate	300 K	42 mm	74 W · m ⁻²	46 W · m ⁻²	-16 W · m ⁻²
isothermal	300 K	42 mm	63 W · m ⁻²	36 W · m ⁻²	-26 W · m ⁻²
lumped	300 K	42 mm	65 W · m ⁻²	36 W · m ⁻²	-29 W · m ⁻²
lapse-rate	310 K	42 mm	53 W · m ⁻²	26 W · m ⁻²	-36 W · m ⁻²
isothermal	310 K	42 mm	42 W · m ⁻²	15 W · m ⁻²	-47 W · m ⁻²
lumped	310 K	42 mm	42 W · m ⁻²	13 W · m ⁻²	-52 W · m ⁻²

Appendix G - HDPE Thickness

s/h	ω	T_A	H ₂ O	$T = 310$ K	$T = 300$ K	$T = 290$ K
4.0	76.0°	290 K	25 mm	81 W · m ⁻²	59 W · m ⁻²	39 W · m ⁻²
4.0	76.0°	300 K	35 mm	61 W · m ⁻²	39 W · m ⁻²	19 W · m ⁻²
4.0	76.0°	300 K	45 mm	56 W · m ⁻²	34 W · m ⁻²	14 W · m ⁻²
8.0	82.9°	290 K	25 mm	100 W · m ⁻²	72 W · m ⁻²	47 W · m ⁻²
8.0	82.9°	300 K	35 mm	75 W · m ⁻²	47 W · m ⁻²	22 W · m ⁻²
8.0	82.9°	300 K	45 mm	69 W · m ⁻²	41 W · m ⁻²	16 W · m ⁻²
16.0	86.4°	290 K	25 mm	110 W · m ⁻²	80 W · m ⁻²	52 W · m ⁻²
16.0	86.4°	300 K	35 mm	82 W · m ⁻²	52 W · m ⁻²	24 W · m ⁻²
16.0	86.4°	300 K	45 mm	75 W · m ⁻²	45 W · m ⁻²	17 W · m ⁻²

Replacing the 13 μm sheet of HDPE with a 100 μm sheet reduces cooling power more than 10 %:

s/h	ω	T_A	H ₂ O	$T = 310$ K	$T = 300$ K	$T = 290$ K
4.0	76.0°	290 K	25 mm	71 W · m ⁻²	52 W · m ⁻²	34 W · m ⁻²
4.0	76.0°	300 K	35 mm	54 W · m ⁻²	35 W · m ⁻²	17 W · m ⁻²
4.0	76.0°	300 K	45 mm	49 W · m ⁻²	30 W · m ⁻²	13 W · m ⁻²
8.0	82.9°	290 K	25 mm	87 W · m ⁻²	63 W · m ⁻²	42 W · m ⁻²
8.0	82.9°	300 K	35 mm	65 W · m ⁻²	42 W · m ⁻²	20 W · m ⁻²
8.0	82.9°	300 K	45 mm	60 W · m ⁻²	36 W · m ⁻²	15 W · m ⁻²
16.0	86.4°	290 K	25 mm	96 W · m ⁻²	70 W · m ⁻²	46 W · m ⁻²
16.0	86.4°	300 K	35 mm	72 W · m ⁻²	45 W · m ⁻²	21 W · m ⁻²
16.0	86.4°	300 K	45 mm	66 W · m ⁻²	40 W · m ⁻²	16 W · m ⁻²

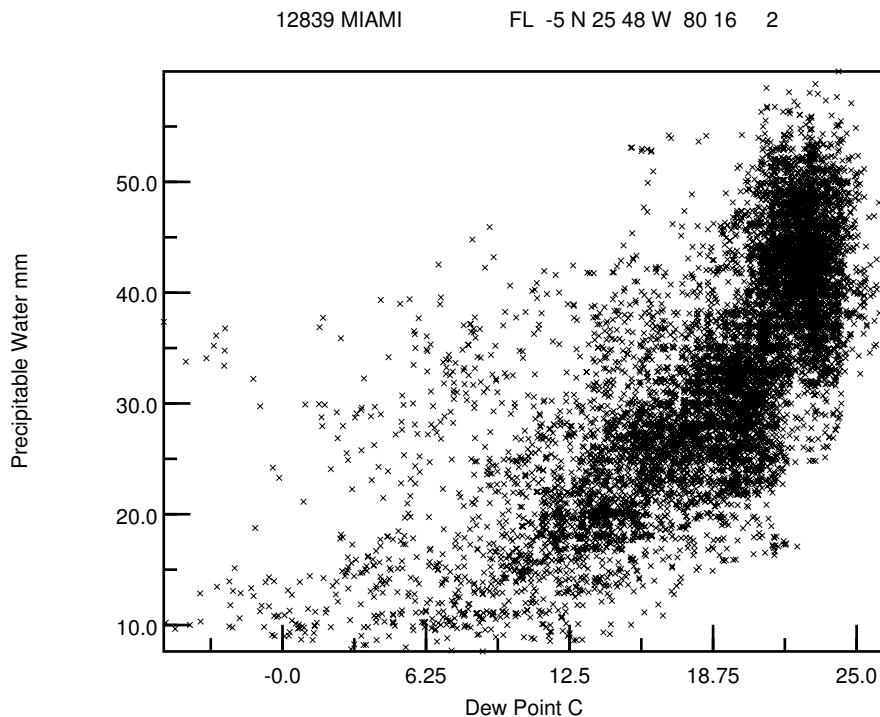
Appendix H - Precipitable Moisture

In “Estimating Moisture Profiles Using a Modified Power Law” [43], Raymond writes: “*Measurements from the GOES-8 and -10 (Geostationary Operational Environmental Satellite) sounders and the SSM/I (Special Sensor Microwave Imager) are used to determine the integrated water vapor or precipitable water. Additionally, brightness (or equivalent blackbody radiation) temperatures associated with GOES sounder water vapor bands 10, 11, and 12, which are centered at 7.4, 7.0, and 6.5 μm , respectively, provide additional information in the vertical. These observations correspond to low-, middle-, and high-level estimates of the relative humidity in the troposphere.*”

The TMY2, Typical Meteorological Year [34], is unusual among climatic data formats in that it contains a field “Precipitable Water” (columns 124 - 128). Total precipitable moisture is a key parameter determining the radiative cooling power available. All the formats contain dew-point or other measures of humidity at ground level. Several investigators have explored the relationship between ground level humidity and precipitable water.

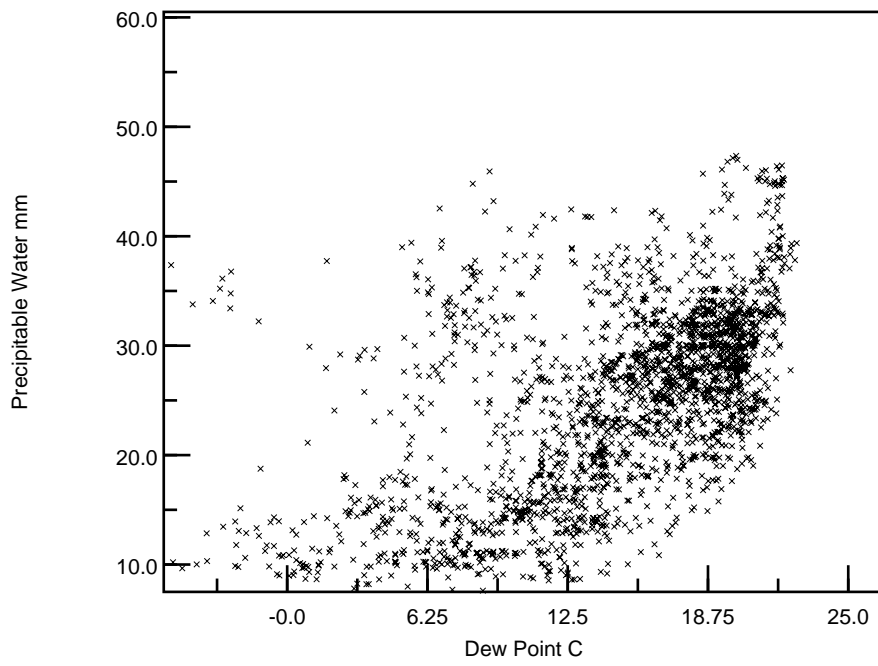
In “Surface Dew Point and Water Vapor Aloft” [40], Reitan finds a high correlation between mean monthly surface dew-point and mean monthly total precipitable water at each of 15 localities in the United States of America. In “Note on the Relationship Between Total Precipitable Water and Surface Dew Point” [41], Smith tries to extend this relationship to daily and hourly values by specializing parameters for latitude and season.

A scatterplot of precipitable moisture versus dew-point temperature shows that, on an hourly basis, precipitable moisture is poorly correlated with ground level humidity in Miami Florida.

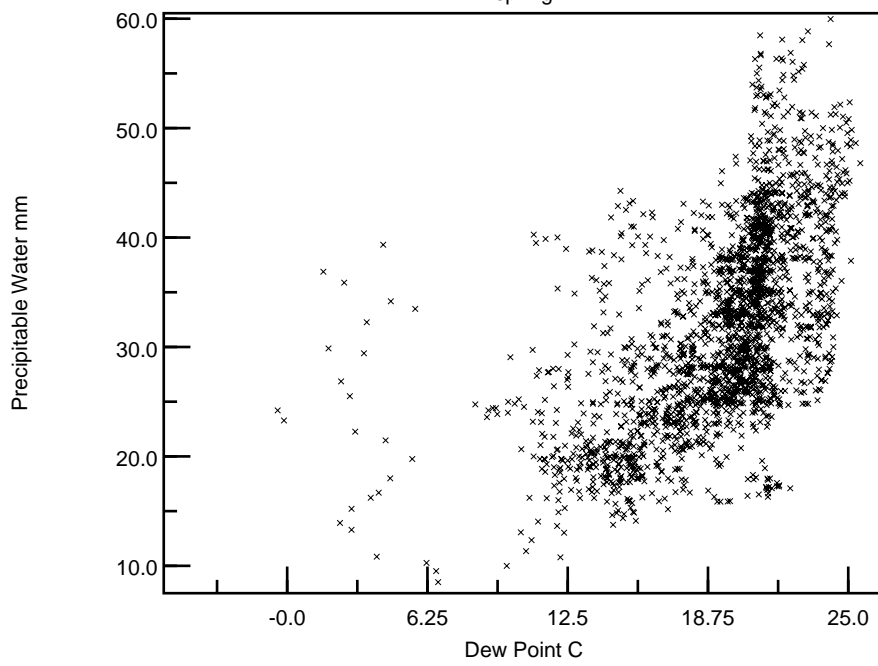


Breaking down by season, the scatterplot for summer is remarkably concentrated around a dew-point of 22 C. However, all the plots show that dew-point temperature in itself is not sufficient for predicting precipitable moisture.

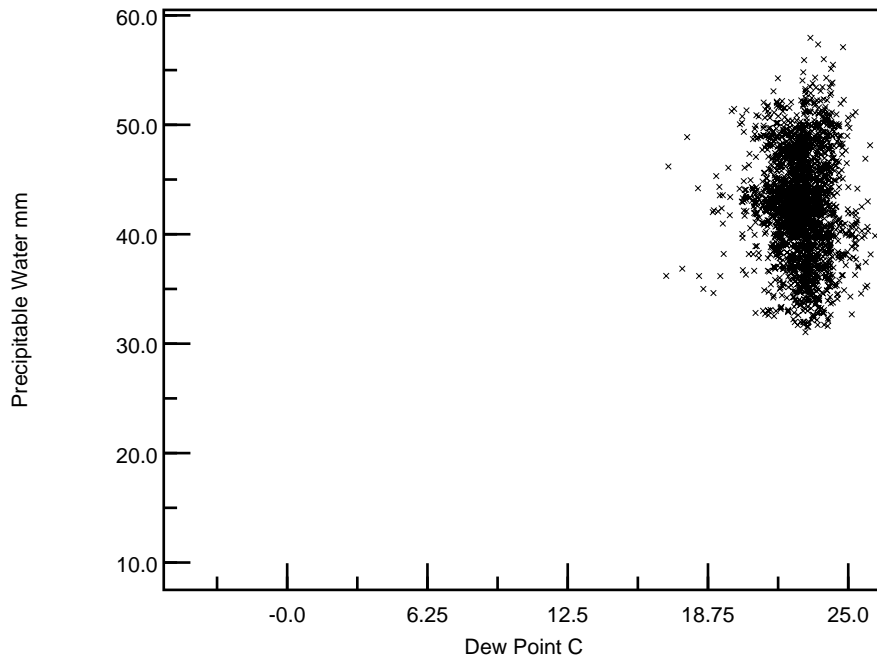
12839 MIAMI FL -5 N 25 48 W 80 16 2
winter



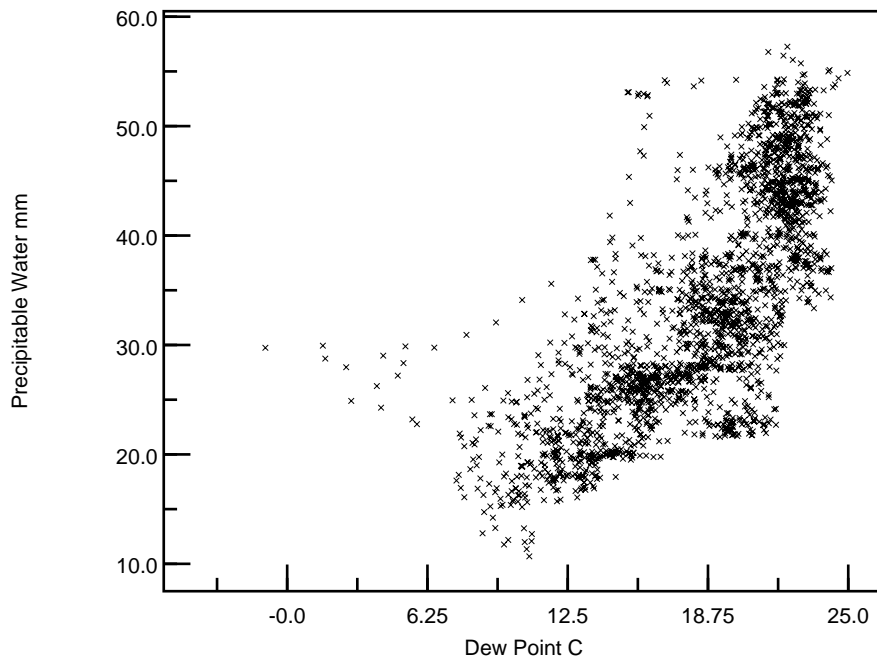
12839 MIAMI FL -5 N 25 48 W 80 16 2
spring



12839 MIAMI FL -5 N 25 48 W 80 16 2
summer



12839 MIAMI FL -5 N 25 48 W 80 16 2
autumn



“Estimating Moisture Profiles Using a Modified Power Law” [43] concludes: “*The results of the present study demonstrate that the estimates of precipitable water from mean monthly surface dew-point temperature are not sufficiently reliable to justify making surface measurements to infer existing preceptitable water.*”